DEVELOPMENT AND EXPERIMENTAL VERIFICATION OF FE-MODEL FOR STRINGER-STIFFENED FIBRE COMPOSITE PANELS UNDER COMBINED THERMAL AND MECHANICAL LOADING CONDITIONS

Raimund Rolfes, Stefan Tacke, Rolf Zimmermann

[1]DLR, Institute of Structural Mechanics
Lilienthalplatz 7, 38108 Braunschweig, Germany
Phone: +49 531 295 2305, Fax: +49 531 2232,
E-mail: raimund.rolfes@dlr.de

ABSTRACT

In this paper a buckling design rule for stringer stiffened curved CFRP panels subjected to combined mechanical and thermal loading is derived by parametric studies with the finite element system ANSYS. At first a finite element model to simulate the buckling behaviour of such panels is established and validated with test results from a former study. Then loading and boundary conditions are adapted to those of the Thermex B testing site at DLR in Braunschweig, and results of linear bifurcation analyses with constant material properties under combined mechanical and thermal load are presented. Additional nonlinear computations with temperature dependent material properties confirm the results of the linear computations. The results of all computations are summarized as the design rule looked for, and then verified by tests.

MOTIVATION AND INTRODUCTION

Space structures in general are high performance structures of low mass and high reliability. Minimisation of mass leads to thin-walled structures, which under compression or shear loading are endangered by buckling. The loading may be of mechanical or thermal type. The choice of rules for designing space structures is indispensable in order to find out the best compromise between the conflicting requirements of low mass and high reliability already in an early design stage. There is a strong need for design rules with respect to buckling caused by combined mechanical and thermal loading. The aim of this research is to develop such rules for characteristic structural components made of CFRP, because the literature studied (e.g. [1] to [5]) does not yield them. The well known finite element system ANSYS is used for that purpose.

As characteristic structural components, curved stringer-stiffened CFRP (carbon fibre reinforced plastic) panels under uniaxial compression from mechanical and thermal loading are chosen since they are typical structural components of future launchers. For other applications like supersonic commercial transport aircraft flat panels might be more appropriate. However this requires other design rules since the curvature is kept constant within the present study.

FINITE ELEMENT MODELLING

In order to establish a finite element model representing the actual behaviour of a real panel, computations have to be performed and compared with test results. For that purpose results of stringer stiffened curved CFRP panels subjected to pure mechanical loading are used. They had been already tested at the large buckling test facility of the Institute of Structural Mechanics as part of a former study, and they were designed pertinent to the requirements of high buckling load and global buckling mode. These so-called ´validation panels´ were cut out of a filament wound cylinder consisting of Vicotex-M18/HTA7 material, and were stiffened afterwards with six equally spaced stringers of the same material. For the buckling tests the loaded edges of the validation panels were clamped and the free longitudinal edges were equipped with a buckling support to prevent wrinkling. The test results are summarized in Table 1.

The finite element model is generated to simulate the deformational behaviour and to reveal buckling loads close to those of the validation panels. The ANSYS model is generated with layered shell elements (Shell 91), consisting of several unidirectional layers with different orientations. Layered volume elements (Solid46) are not considered, because they do not incorporate the plane stress state of a thin shell and because the shear distribution across the thickness of an element is assumed constant. The layered shell element (Shell 91) is expected to predict the stress state of a thin shell correctly, and it enables the use of nonlinear material behaviour for each layer, e.g. matrix softening at elevated temperatures. This will be important for nonlinear computations with combined mechanical and thermal load.

Special care has to be taken in the modelling of the connection between stringer flanges and skin. Models that incorporate the stiffness of the stringer flanges in the skin reveal computational problems and incomparable results. The results improve when the stiffness of the

stringer flanges is separated from the skin and modelled as a distinct element on a different radius. Afterwards the elements of the stringer flanges and the skin have to be connected to gain the correct stiffness of the whole structure.

Simple coupling of the degrees of freedom (DOF), this means that translations and rotations of adjacent nodes at a different radius are set to become equal, leads to a weak structure, because the interaction between rotations and translations of connected elements which are located on different radii is not considered. The use of beam elements (Beam 4) between the adjacent nodes is a good way to model the real connection between stringer flanges and skin, as the interaction of rotations and translations is taken into account (Fig. 1, Sketch a). The FE-model becomes much stiffer and reveals improved computational results.

The computed buckling loads and modes are strongly affected by the loading and boundary conditions of the finite element model. As the validation panel is clamped at the loaded edges, the circumferential and the out of plane displacements at these edges of the model are set to zero (v,w = 0, Fig. 2). One end of the panel is fixed (u_{lo} = 0) and the load is introduced by a given displacement at the other end (u_{lu} = def.). At the longitudinal edges of the validation panels a buckling support to prevent wrinkling is fixed. The assumption w = 0 in this area leads to a very stiff structure, because the panel then behaves like being fixed in a stiff frame. The problem is overcome by coupling of the rotational DOF of the nodes in the regions of the buckling support (rotx = const., roty = 0, $u_{y=const.}$ = const.; Fig. 2). So these areas act like rigid structures with allowed out of plane movements of the whole area (see Fig. 3).

Linear bifurcation analyses are performed with the model of the validation panel for mechanical loading only. As the theoretical eigenvalue of the perfect structure is computed, the resulting buckling loads have to be higher than the measured ones, which belong to imperfect structures (conf. Table 1).

Nonlinear analyses are performed in order to obtain buckling loads depending on geometric and material nonlinearities. Combined loads can be used and changed independently of each other, e.g. axial shortening can be changed with a fixed temperature distribution to gain a critical state with respect to thermal load.

The calculation is done with a wavefront solver using a Newton-Raphson iteration scheme and back-substitution for solution. To deal with the geometric and material nonlinearities the load has to be applied incrementally in several substeps. Each substep consists of additional equilibrium iterations, in which the tangent stiffness matrix of the structure is updated and the convergence of the calculation is checked. The computation stops automatically if the equilibrium iterations fail to converge. This point is considered as the nonlinear buckling load of the structure. From the analytical point of view there is no guarantee not to overlook critical states. However, as the model is verified by real tests, this issue is not considered an actual problem.

A perfect structure as well as a structure with initial imperfections are studied. As usual in buckling computations, the imperfection shape is chosen to coincide with the first eigenmode. Several computations with different amplitudes of the imperfection reveal that the best numerical behaviour is attained with an amplitude of δz = 0.2 mm (which is 13% of the skin thickness). Imperfections with a minor amplitude do not affect the buckling behaviour and imperfections with a greater amplitude dominate it. The nonlinear buckling loads are given in Table 1. Comparing experimental and numerical results shows that the nonlinear buckling load is in very good agreement with the maximum experimental buckling load.

INFLUENCE OF LAMINATE SET-UP AND THERMAL LOADING

The validated FE-model is in principle used for deriving the design rule. However, since this rule was planned to be verified by at least one test under combined thermal and mechanical loading within the Thermex B test site, the model has to be adjusted to the geometry and boundary conditions of this facility. Especially the clamping conditions at the loaded edges are different from those of the large buckling test facility; the clamping boxes are divided into several segments allowing transverse deformation of the test panel. Therefore the areas of the FE-model with the boundary conditions reflecting the clamping are changed in their length, and a separate coordinate system for these boundaries is defined to allow transverse deformations δv (conf. Figure 2 for the coordinate system). Then parametric studies are performed to derive the design rule; the lay-up and the thermal loading are chosen as variables. Some of the stacking sequences investigated are given in Table 2.

In order to apply a thermal load to the structural model of the panels, a thermal model to calculate the temperature distribution is developed. It consists of thermal solid elements (Solid70) with temperature as the only degree of freedom. Temperatures on the outer surface of the panel are directly applied to the FE-nodes, as a predefined temperature will be applied in the real tests. On the inner side of the panel a free convection is applied to the element surfaces, as the test panel will be cooled by convection with air.

Since the structural model consists of shell elements the computed temperature distributions of the thermal model can not be used directly for thermal loading of the structural model. To overcome this problem a special ANSYS post-processing procedure is created. This procedure requires a thermal model with exactly the same finite element size and element numbering as the structural model. The computed temperature distribution

of every thermal solid element is used within this procedure to write a command file with thermal loads for every layer of the corresponding layered shell element of the structural model. In a structural analysis this command file is read and the structural model is thereby loaded thermally. This cumbersome transference of temperatures can be avoided if advanced finite shell elements for heat transfer in composite structures can be used [6]. They should be implemented into standard FE-packages like ANSYS.

Two different temperature distributions are regarded.

1) On the outer surface of the panel the limit temperature of the used matrix system of T_{out} = 150 °C is applied, and on the inner side of the panel a free convection with air of T_{air}= 25 °C is assumed. The convection coefficient on the inner side of the panel is varied to achieve a temperature distribution as measured in preliminary thermal tests with a temperature gradient of ΔT_{skin} = -8 °C across the thickness of the skin and ΔT_{str} = -44 °C across the stringer height. The convection coefficients come to be k = 20 W/Km² for the inner surface of the panel skin area between the stringer feet, k = 15 W/Km² for the stringer feet area, and k = 3 W/Km² for the stringer blade.

2) On the outer surface of the panel the limit temperature of the used matrix system of T_{out} = 150 °C is applied, and on the inner side of the panel a free convection with cryogenic temperatures of T_{cryo} = -200 °C is assumed. The convection coefficient for the boiling liquid nitrogen is estimated to be about k = 5000 W/Km² according to literature. This results in a temperature gradient across the thickness of the skin of ΔT_{skin} = -334 °C and to ΔT_{str} = -350 °C across the height of the stringer blade.

In the structural computations with thermal load the same temperature distribution is used for all laminate set-ups of the skin. This is permissible, as the heat flow in the panel is normal to the fibre orientation and therefore independent of it, and as the temperature distribution in longitudinal direction is assumed constant.

The loading of the test panel model with temperature distribution 1 and fixed clampings results in axial compressive forces of about F_{th} = -2 kN for most of the lay-ups (not all shown in Table 2). Typical out of plane deformations range from δw = -0.03 mm to δw = +0.1 mm. Exceptional to this are the lay-ups 4-5 and 7-8, which reveal axial tensile forces from F_{th} = 1.26 kN up to F_{th} = 6 kN. These forces are caused by the contraction of the panel due to the high contribution of fibres to the behaviour in axial direction of the panel in combination with the negative thermal expansion coefficient in fibre direction. The out of plane deformations range from δw = -0.006 mm to δw = +0.04 mm and from δw = -0.019 mm to δw = +0.046 mm, respectively.

Some laminate lay-ups (7-8,18-19) are loaded with the temperature distribution 2) as well, because they reveal a high buckling load in combination with either a large contraction (7-8) or a large expansion (18-19) under the thermal distribution 1. The tensile force of the lay-ups 7-8 decrease from F_{th}= 6 kN (temperature distribution 1) to F_{th} = 3.5 kN. For the lay-ups 18-19 the axial compressive force increase from F_{th} = -1.86 kN (temperature distribution 1) to F_{th} = -3.65 kN, but the out of plane deformations decrease to just the half. This behaviour is caused by the stringers as they expand in axial direction due to the cryogenic cooling (negative thermal expansion coefficient).

Mechanical buckling loads of about F_B = -200 kN are considered (cf. Table 2). So the additional thermally induced compression of about F_{th} = -2 kN to F_{th} = -3.65 kN due to the temperature distributions (1) and (2) can be neglected. For the lay-ups 4-5 and 7-8 thermal load even leads to a small relaxation at a prescribed shortening of the panel. Computational experience shows, that the out of plane deformations are very small. Although these results indicate already a small influence of the thermal loading part on buckling behaviour, linear bifurcation analyses with combined thermal and mechanical load are performed. This analysis computes eigenvalue scaling factors for the stress state of a prestressed structure. In the combination of thermal load and different axial shortening, the share of thermally induced stress at the prestressing force can be changed (tiny axial shortening - thermal prestressing dominates; large axial shortening - structural prestressing dominates).

For a given shortening and temperature distribution, the computed scaling factor for the prestress state belongs to the shortening as well as to the entire temperature distribution. As at prestressing the axial force is computed, the scaling factor can be used to evaluate the bifurcation buckling load dependent upon the scaled shortening and scaled temperature distribution.

The computations are shown for the lay-up of the test panel (1), one lay-up of high mechanical buckling load (13) and a lay-up of minor mechanical buckling load (4), Figures 4-6. Additionally laminates with an extreme axial thermal contraction (23) and an extreme axial thermal elongation (26) are studied, to determine maxima in the influence of thermal loading on buckling load, Figures 7-8. For the sake of better understanding the maximum temperature of the scaled temperature distribution is added at several points in the figures.

In Figures 4-8 the buckling load is shown in relation to the pre-stress state. The buckling load for pure mechanical loading is independent of the mechanical pre-shortening of the panel. For combined thermal and mechanical loading the buckling load decreases only for tiny mechanical pre-shortenings. In these cases the thermal load dominates the pre-stress state of the structure. But to reach the bifurcation buckling load large scaling factors are computed, and this results in extreme temperatures needed for buckling.

The Figures 7 and 8 for the lay-ups 23 and 26, which yield extreme axial thermal contraction and extreme axial thermal elongation, respectively, clearly demon-

strate, that the buckling loads even for an extreme thermal behaviour decrease only at very high temperatures, Figure 8, or slightly increase, Figure 7.

These results of linear bifurcation computations demonstrate, that for a reduction of the buckling load temperatures are needed (about 1000°C), that are out of range of the material possibilities. In the considered range of temperatures (limit temperature of 150 °C) a structurally well designed lay-up like the used one for the test panels, can resist these additional temperatures without any remarkable decrease in buckling load.

Before formulating the design rules the results obtained by the linear computations are checked by computations for the test panel (no. 1 in Table 2), which take into account nonlinear effects. A new off-set feature of the Shell91-element eases up the modelling and reduces the computing time. In the standard formulation of shell elements, the nodes of the element are located at its midplane, whereas the new feature of the layered shell element Shell91 enables the user to move the nodes to the surfaces of the element. The nodes of the panel skin elements are located at the inner side of the panel and the nodes of the stringer feet are located at the bottom of these elements (Figure 1, sketch b). So the nodes of the skin elements and of the stringer feet elements are located on the same radius and in fact at identical positions. This way the same nodes can be used for the skin and for the stringer feet elements. The need for connecting the nodes with beam elements no longer exists. This new formulation reduces the computational time to about 50 % with no changes in buckling loads. Slightly different material properties (conf. Table 3) as for the linear analysis are used. Thus the subsequent buckling loads cannot be compared directly with the ones indicated in Table 2.

Nonlinear computations with the perfect test panel geometry reveal deformations of the form of the second eigenmode and buckling occurs slightly below the load of the second mode. Additional thermal loading even increases the buckling load. To initiate buckling in the expected first mode at minor loads, imperfections of the form of the first eigenmode (2 halfwaves, worst case) with an amplitude of $\delta z = 0.1$ mm are used. This amplitude is sufficient to initiate buckling in the nonlinear analyses.

A nonlinear computation of the imperfect model without thermal load results in a buckling load of F_B = -185.22 kN at a shortening of δz = -2.48 mm. Additional thermal loading with temperature distribution 1 results in almost exactly the same buckling load of $F_{B,th1}$ = -185.23 kN at a shortening of δz = -2.38 mm (conf. Table 4). The temperature gradient of distribution 2 even increases the buckling load to $F_{B,th2}$ = -197.92 kN at a shortening of δz = -2.63 mm.

As the thermal prestressing of the structure is higher with the temperature distribution 1, -6.29 kN compared to -1.89 kN of 2, this effect relies only upon the initial deformation due to the thermal load. The deformations of the panel loaded with temperature distribution 1 are negligibly small, whereas the temperature distribution 2 reduces the radius locally at two positions. This stiffens the panel and increases the buckling load.

The computations considering nonlinear effects confirm the results of the linear computations. The buckling behaviour of well designed curved, stringer stiffened CFRP panels of the assumed material is practically not affected by additional thermal loads. Thus, the resulting buckling design rule is:

Buckling of structurally well designed stringer stiffened curved CFRP panels subjected to combined mechanical and thermal load is practically not affected by the thermal load part. Therefore the thermal contributions to loading can be neglected, and the panels need to be designed with respect to buckling only by consideration of mechanical loading.

EXPERIMENTAL VERIFICATION

Two nominally identical panels from Fiberite 954-2A/IM7, provided by SABCA, are tested in DLR´s THERMEX B test facility. The stacking is given by set-up 1 of Table 2, and the temperature dependent material data can be taken from Table 3. Panel A is subjected to pure mechanical loading under room temperature until buckling. Since the panel is damaged in this test, panel B is used for the combined thermo-mechanical test. Previously panel B was also subjected to pure mechanical loading until 90% of the buckling load of panel A. Strain gage results indicate that both panels have the same stiffness, and at 90 % of the load, buckling has to be expected soon. Thus, the buckling loads of both panels under pure mechanical load are considered to be very close together. Panel B is then thermally loaded up to the limit temperature of 150 °C (temperature distribution 1) and compressed until buckling. The agreement of the experimental buckling loads with the numerical predictions by the nonlinear calculations including imperfections is extremely good (conf. Table 4). Figure 9 shows that also the buckling modes compare very well.

SUMMARY

A buckling design rule for stringer stiffened curved CFRP panels subjected to combined mechanical and thermal loading is derived from results of parametric studies. These are performed by means of finite element computations using the ANSYS system. The finite element modelling is carefully established and verified by comparison with existing test results, in particular attention is given to adequate modelling of skin stringer connections and experimental boundary conditions. The derived derign rule means, that the CFRP panels under consideration can be designed against buckling by dealing with the mechanical load part only. Tests with mechanical and thermal loading confirm this finding. Fur-

ther research is required for flat panels and different boundary conditions.

ACKNOWLEDGEMENT

Funding of the work by ESA/ESTEC within FESTIP is gratefully acknowledged. Two test panels together with material data were provided by SABCA.

REFERENCES

[1] L.X. Sun and T.R. Hsu: *Thermal buckling of laminated composite plates with transverse shear deformation,* Computers and Structures 36 (1990) 883-889

[2] A.K. Noor: *Thermomechanical buckling and postbuckling of multilayered composite panels*, AIAA Paper 92-2541

[3] K. Rohwer: *A further study on thermal buckling of simply supported antimetric angle-ply laminates in a uniform-temperature field,* Composite Science and Technology, vol.46, no.1, 1993, 85-86

[4] A.K. Noor and W.S. Burton *Three-dimensional solutions for the thermal buckling and sensitivity derivates of temperature-sensitive multilayered angle-ply plates,* Transaction J. of Applied Mechanics, vol.59, no.4, Dec 1992, 848-856

[5] C.A. Meyers and M.W. Hyer*: Thermal buckling of symmetrically laminated composite plates,* Mechanics of composites at elevated and cryogenic temperatures Proc. Symposium, ASME Applied Mechanics Conf., Columbus, OH June 16-19 1991; NY, ASME, 1991, 287-303

[6] Rolfes, R.; Noack, J.; Taeschner, M.: *High Performance 3D-Analysis of Thermo-Mechanically Loaded Composite Structures*, in: Atluri, S.N.; O´Donoghue, P.E.: Modeling and Simulation Based Engineering, Proceedings of the International Conference on Computational Engineering Science, Atlanta, Tech Science Press, Palmdale, 1998, 315-320

TABLES AND FIGURES

Table 1: Results for the validation panel

$F_{B,aver}$	-173.17kN	Tests
Δx_{aver}	2.85mm	
$F_{B,max}$	-208.08kN	
Δx_{max}	3.38mm	
$F_{B,bifu}$	-267.32kN	Linear Analysis
Δx_{bifu}	4.23mm	
F_{perf}	-236.42kN	Nonlinear Analyses
Δx_{perf}	3.73mm	
F_{imp}	-213.59kN	
Δx_{imp}	3.38mm	

Table 2: Separated mechanical and thermal analysis

	Set-up of layers	Buckling loads [kN]	Thermal pre-load 1 [kN]	Thermal pre-load 2 [kN]
1.	((+-45)2,90,0)s	-198.57 ; -276.76	-1.170	
4.	(+- 45)3s	-159.48 ; -237.78	1.260	
5.	(+-45)6	-159.23 ; -238.22	1.070	
7.	((0)2,(+-45)2)s	-200.49 ; -203.10	5.846	3.5
8.	((+-45)2,(0)2)s	-225.00 ; -281.81	6.046	3.5
13.	((90)2,(0)2,+-45)s	-229.91 ; -276.57	-2.744	
18.	(90,+-30)2s	-220.54 ; -300.49	-1.843	-3.65
19.	((90)2,(+-30)2)s	-231.33 ; -269.85	-1.855	-3.65
23.	(+-45,(0)4)s	-222.21 ; -222.81	10.098	
26.	((90)4,+-45)s	-175.85 ; -206.70	-9.763	

Table 3: Material properties

	Room temperature	150 °C
$E_{11,t}$	156 GPa	166 GPa
$E_{22,t}$	9.2 GPa	7.4 GPa
$E_{11,c}$	155 GPa	160 GPa
$E_{22,c}$	9 GPa	not obtained
ν_{12}	0.34	0.30

Table 4: Comparison of buckling loads

	Calculation	Experiment
Pure mechanical load	208.30 (linear) 185.22 (nonlinear)	182.0
Additional thermal load 1	185.23 (nonlinear)	175.8

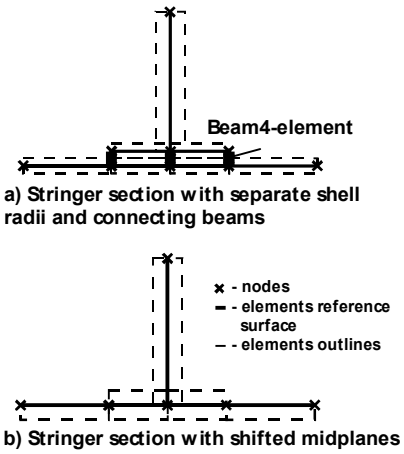

Fig. 1: Stringer section discretisation

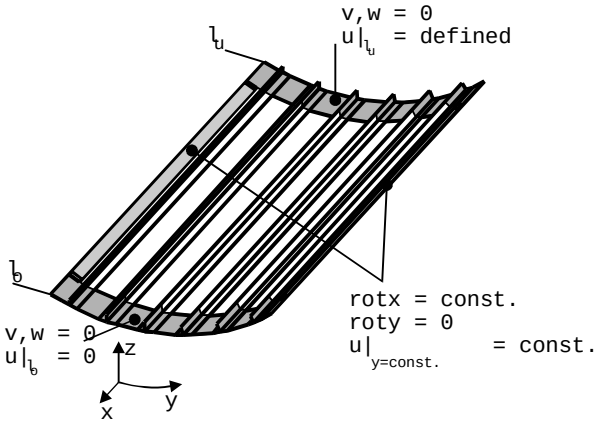

Fig. 2: Coordinate system and boundary conditions

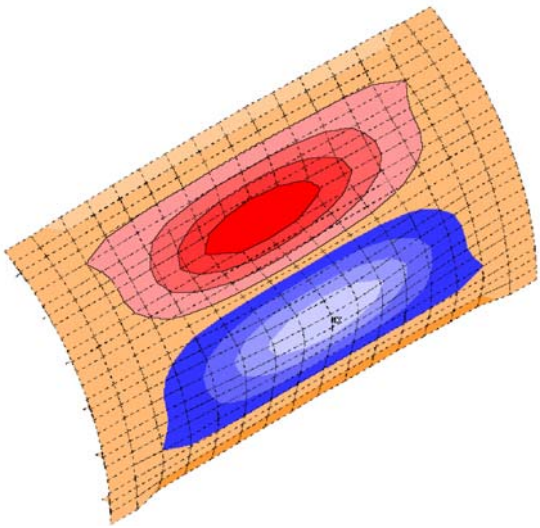

Fig. 3: Buckled validation panel

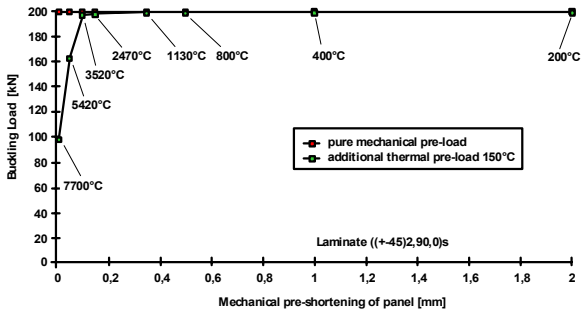

Fig. 4: Buckling load depending on pre-stress state, laminate 1 (test panel)

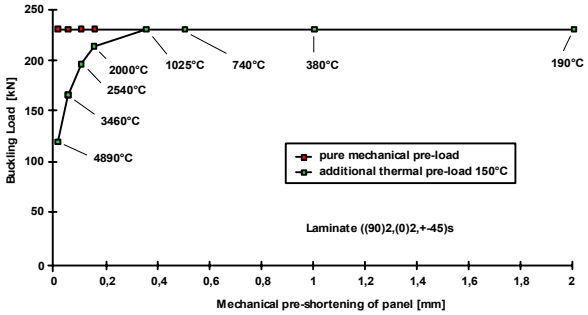

Fig. 5: Buckling load depending on pre-stress state, laminate 13 (high mechanical buckling load)

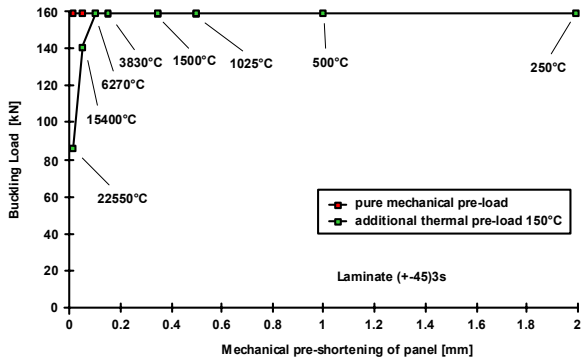

Fig. 6: Buckling load depending on pre-stress state, laminate 4 (low mechanical buckling load)

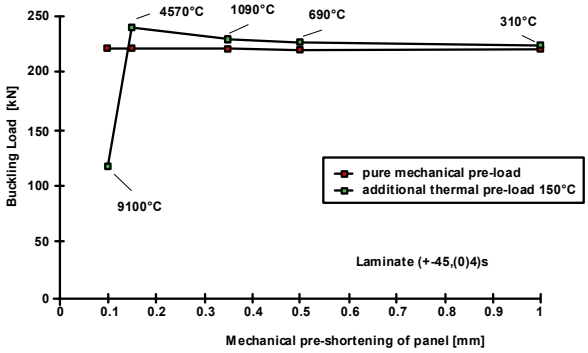

Fig. 7: Buckling load depending on pre-stress state, laminate 23 (extreme thermal contraction)

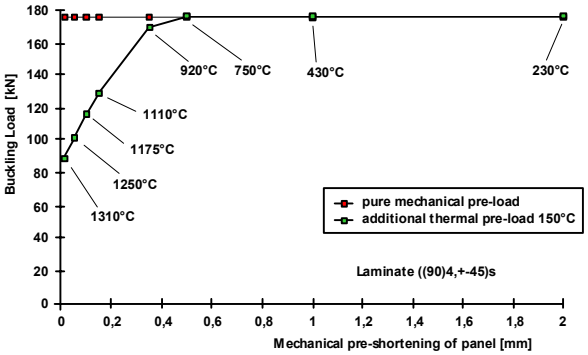

Fig. 8: Buckling load depending on pre-stress state, laminate 26 (extreme thermal elongation)

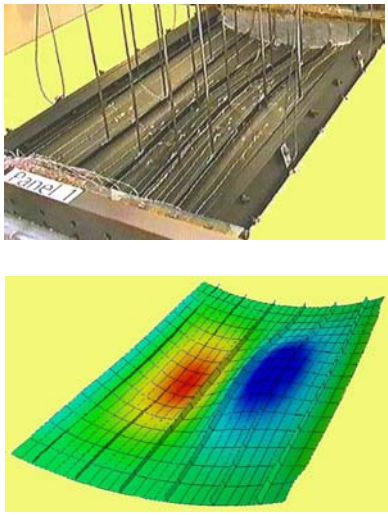

Fig. 9:Experimental and calculated buckling mode